Seed localization in Ultrasound and Registration to C-Arm Fluoroscopy Using Matched Needle Tracks for Prostate Brachytherapy

Mehdi Moradi*, *Member, IEEE*, S. Sara Mahdavi, *Student Member, IEEE*, Ehsan Dehghan, Julio R. Lobo, Sanchit Deshmukh, William James Morris, Gabor Fichtinger, *Member, IEEE*, and Septimiu (Tim) E. Salcudean, *Fellow, IEEE*

***Abstract*—We propose a novel fiducial-free approach for the registration of C-arm fluoroscopy to 3-D ultrasound images of prostate brachytherapy implants to enable dosimetry. The approach involves the reliable detection of a subset of radioactive seeds from 3-D ultrasound, and the use of needle tracks in both ultrasound and fluoroscopy for registration. Seed detection in ultrasound is achieved through template matching in 3-D radio frequency ultrasound signals, followed by thresholding and spatial filtering. The resulting subset of seeds is registered to the complete reconstruction of the brachytherapy implant from multiple C-arm fluoroscopy views. To compensate for the deformation caused by the ultrasound probe, simulated warping is applied to the seed cloud from fluoroscopy. The magnitude of the applied warping is optimized within the registration process. The registration is performed in two stages. First, the needle track projections from fluoroscopy and ultrasound are matched. Only the seeds in the matched needles are then used as fiducials for point-based registration. We report results from a physical phantom with a realistic implant (average postregistration seed distance of 1.6 $\pm$ 1.2 mm) and from five clinical patient datasets (average error: 2.8 $\pm$ 1.5 mm over 128 detected seeds). We conclude that it is feasible to use RF ultrasound data, template matching, and spatial filtering to detect a reliable subset of brachytherapy seeds from ultrasound to enable registration to fluoroscopy for dosimetry.**

***Index Terms*—Prostate brachytherapy, template matching, ultrasound imaging, X-ray fluoroscopy.**

I. Introduction

LOW dose rate brachytherapy is a minimally invasive therapeutic procedure for prostate cancer that has rapidly gained acceptance due to highly successful clinical outcomes [1]. In brachytherapy, a number of cylindrical radioactive sources or seeds (^{125}I or ^{103}Pd), of length 4.5 and diameter of 0.8 mm are permanently implanted into the prostate using needles. The aim is to deliver a sufficient radiation dose to kill cancerous tissue while limiting the dose in radio-sensitive regions such as the bladder, urethra, and rectum. Transrectal ultrasound (TRUS) is used to intraoperatively guide the transperineal insertion of the needles. As a result of the motion of the gland due to needle forces and possible intraoperative changes to the plan due to interference with the pubic arch or lack of implantable tissue, the locations of the implanted seeds do not necessarily match the initial treatment plan. Hence, for quality assurance, intraoperative dosimetry is highly beneficial [2]. As a result, enabling technologies for intraoperative planning or plan modification have received significant attention from the medical imaging community [3].

Several groups have approached ultrasound-based seed detection [4]–[7]. However, accurate seed localization based on ultrasound has proven to be a very difficult task due to clutter from other highly reflecting objects such as calcifications resulting in false positive appearances, seed specularity, and shadowing, and limited field of view. Even when hand segmented, up to 25% of the seeds remain hidden in ultrasound images [8]. Therefore, C-arm fluoroscopy is commonly used for visual assessment of the implanted seeds. However, the prostate gland is not discernible in fluoroscopy images. Fusion of the fluoroscopy images and ultrasound is therefore considered as a possible solution [9]–[12]. If complete seed localization and implant reconstruction from fluoroscopy images are available, the registration of the result to the ultrasound images will enable dosimetry. Recently, the fluoroscopy seed detection [13], [14]

Manuscript received January 9, 2012; revised May 7, 2012; accepted June 20, 2012. Date of publication June 29, 2012; date of current version August 16, 2012. This work was supported by National Institutes of Health (NIH) under Grant R21 CA120232. The work of M. Moradi was supported by the Natural Sciences and Engineering Research Council of Canada (NSERC) Postdoctoral Fellowship and a Prostate Cancer Training Award from the U.S. Army Medical Research and Materiel Command under Grant W81XWH-10-1-0201. The work of S. S. Mahdavi was supported by the Prostate Cancer Foundation of British Columbia. The work of G. Fichtinger was supported by Cancer Care Ontario Research Chair. The work of S. E. Salcudean was supported by the Natural Sciences and Engineering Research Council of Canada (NSERC) and the Canadian Institutes of Health Research (CIHR). *Asterisk indicates corresponding author.*

*M. Moradi is with the Department of Electrical and Computer Engineering, University of British Columbia, Vancouver, BC V6T 1Z4, Canada (e-mail: moradi@ece.ubc.ca).

S. S. Mahdavi, J. R. Lobo, and S. E. Salcudean are with the Department of Electrical and Computer Engineering, University of British Columbia, Vancouver, BC V6T 1Z4, Canada (e-mail: saram@ece.ubc.ca; juliol@ece.ubc.ca; tims@ece.ubc.ca).

E. Dehghan was with the Department of Electrical and Computer Engineering, Johns Hopkins University, Baltimore, MD 21218 USA. He is now with the Philips Research North America, Briarcliff Manor, NY 10510 USA (e-mail: ehsand@jhu.edu).

S. Deshmukh is with the Indian Institute of Technology, Bombay 400076, India (e-mail: sanchitd@iitb.ac.in).

W. J. Morris is with the Vancouver Cancer Center, Vancouver, BC V5Z 4E6, Canada (e-mail: jmorris@bccancer.bc.ca).

G. Fichtinger is with the School of Computing, Queen's University, Kingston, ON K7L 3N6, Canada (e-mail: gabor@cs.queensu.ca).

Color versions of one or more of the figures in this paper are available online at http://ieeexplore.ieee.org.

Digital Object Identifier 10.1109/TBME.2012.2206808

and implant reconstruction problems [15] have been extensively addressed. Given three to five fluoroscopy images, and the relative pose of the C-arm in each acquisition, we have reported that the back-projection technique can be used to accurately reconstruct the 3-D implant [15].

Patient and equipment motion between the acquisition of ultrasound and fluoroscopy always exist and need to be compensated in registration. Due to the lack of clinically sufficient accuracy and robustness in seed detection from ultrasound, some authors advise the use of intensity-based methods rather than point-based registration [9]. Also, the use of fiducial markers is an unwelcome addition to the ordinary setup in the operating room due to time and space limitations. Nevertheless, attaching fiducial markers to the ultrasound probe [16] and using the ultrasound probe as a fiducial [10] have been mentioned. To remove the need for fiducials, using the seeds for registration has been reported [17]. For success of point-based registration, there needs to be a small number of false positive seed detections and a reliable initial alignment. Therefore, many investigators have implemented fusion of ultrasound and fluoroscopy for dosimetry based on the tedious task of manual segmentation of seeds in ultrasound [11], [17]. In this paper, we report automatic partial detection of the seed cloud from ultrasound RF data and deformable registration to the fluoroscopy seed cloud.

We present several novel technical contributions. For seed detection, we perform 3-D template matching on *filtered RF data* to enhance strong reflectors. In the registration step, we propose the matching of the *needle tracks* formed by the most reliable ultrasound seeds with fluoroscopy needle tracks. We also propose a *deformable* point-based registration framework that takes advantage of a simple model of the deformation caused by the pressure from the TRUS probe, applied to fluoroscopy images. We hypothesize that given a complete fluoroscopy reconstruction, a small and rigorously filtered subset of seeds extracted from the ultrasound data can be used for sufficiently accurate registration when a needle matching process is performed to provide an initial alignment and the probe-induced deformation is modeled.

The proposed methodology targets a complicated and long standing problem, with very little addition to the routine therapeutic procedure. The results are reported on data collected from five patients during brachytherapy procedures in our institution. The method is also validated on a physical phantom. This paper is organized as follows. In Section II, the ultrasound-based seed detection and filtering approach are detailed and our registration method is described. Section III presents the results of seed detection and registration. Section IV provides our discussions and concludes this paper.

II. Methods

The outline of our methodology is detailed in Fig. 1. For reconstruction of the implant in fluoroscopy, we implemented and used our method previously described in [15]. The fluoroscopic images were acquired from a GE Series 9800 mobile C-arm, while the patient was still in the operating room and under anesthesia. The use of C-arm during brachytherapy is a routine practice in our institution. Three fluoroscopy images were collected

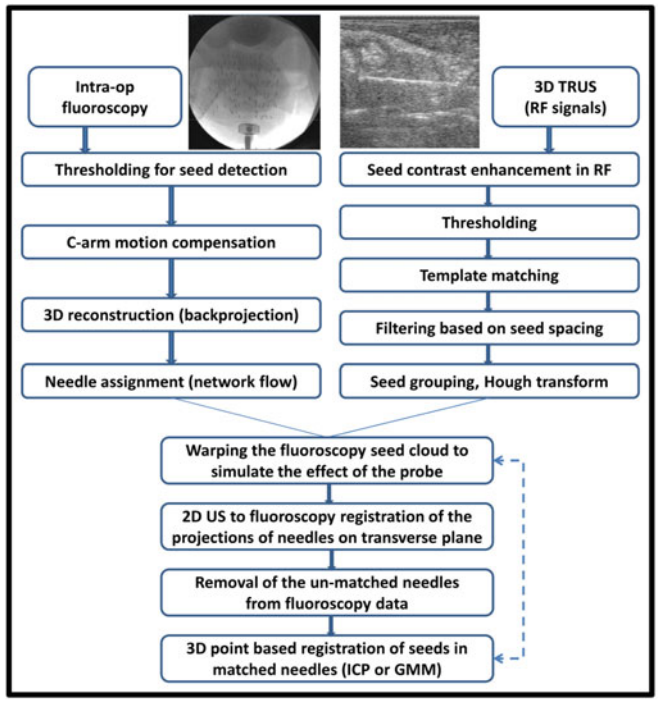

Fig. 1. Workflow of the seed detection method.

at -5°, 0°, and 5° C-arm angles. The fluoroscopy reconstruction steps included C-arm pose estimation from rotation angle and compensation for sagging, followed by finding the 3-D seed positions through minimizing the symbolic distance between back projected lines from seed shadows in the three images. A minimum cost flow technique was used to assign seeds to needles [18]. The resulting reconstruction was compared to the brachytherapy preplan, considering the intraoperative changes, and was confirmed to match the plan in terms of number of seeds and needles, and the seed to needle assignments for all the patient datasets and the phantom data.

In this paper, we focus on ultrasound-based partial seed detection, needle matching, and registration from ultrasound to fluoroscopy. Details of these steps are provided in the following sections.

A. Seed Detection

1) 3-D Ultrasound Setup and Data: We used a custom made 3-D ultrasound data acquisition system based on a brachytherapy stepper (EXII, CIVCO Medical Solutions, Kalona, IA) modified by motorizing the cradle rotation (see Fig. 2). The sagittal array of a dual plane linear/microconvex broadband 5–9 MHz endorectal transducer (Ultrasonix Medical Corpoartion, Richmond, BC, Canada) was used. RF data were recorded at a frame rate of 21 f/s, during the probe rotation from -45° to 50°, where 0° corresponded to the probe aligned with the central sagittal cross section of the prostate gland. The 2-D frame size was $5 \times 5.5\ \text{cm}^2$ and typically 270 sagittal frames were collected for each patient/phantom while the TRUS probe was rotated around the z-axis. We define the z-axis as the longitudinal axis of the probe along the superior–inferior direction of the patient, and the xy plane to be the transverse scan plane.

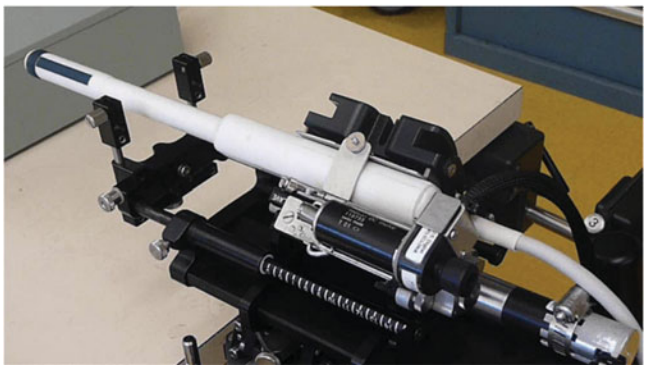

Fig. 2. 3-D ultrasound acquisition setup based on the brachytherapy stepper. The sagittal plane of the TRUS probe is used to acquire images while rotating along the axis.

The typical size of the brachytherapy implant is larger than the size of the field of view of our 3-D ultrasound system. We noted that the far anterior and lateral needles often did not lie within the field of view, making complete ultrasound-based seed detection impossible with a single 3-D scan. Increasing the imaging depth and rotation angle was technical possibilities. However, our goal was to show that the more realistic scenario of partial seed detection in RF ultrasound data is sufficient for registration. With the present single 3-D scan, data acquisition is less than 15 s, and repositioning of the TRUS is not required, making the method suitable for clinical implementation.

We present the results of our study on data collected immediately after seed implantation in the operating room, from five brachytherapy patients. The approval of Research Ethics Board of the University of British Columbia was obtained. Patients provided informed consent. The procedures were performed at the Vancouver Cancer Center. The standard procedure at the VCC is the use of *stranded* seeds for prostate brachytherpay. We also present data from a CIRS Model 053 tissue-equivalent ultrasound prostate phantom (CIRS, Inc., Norfolk, VA). For this phantom, a plan consisting of 135 seeds and 26 needles was created which was carried out by a radiation oncologist.

2) RF Signal Processing: A sagittal RF ultrasound frame in our data consisted of 128 scan lines. In order to improve the seed to background contrast, we averaged the signal power over windowed blocks of the RF signals. In other words, we replaced a segment of length n at depth d of an RF line with the reflected power P_d computed as follows:

$$P_d = \frac{\sum_{k=1}^{n} w(k)x(k)^2}{n} \tag{1}$$

where $x(k)$ $(k = 1, \ldots, n)$ are the samples in the RF segment, and $w(k)$ are Hamming window weights. This step was applied with $n = 6$ and a 50% overlap between consecutive blocks. We have shown that this process doubled the contrast to noise ratio between the seed regions and the background [19]. Furthermore, the resulting reduction in the size of the RF signals improved the speed of the template matching step. The contrast enhancing operation described in (1) was completed in 13 ms for a 2-D frame. A sample of the outcome of this process is illustrated in Fig. 3.

The resulting contrast enhanced 2-D sagittal images were then used to reconstruct a 3-D volume. The 3-D reconstruction

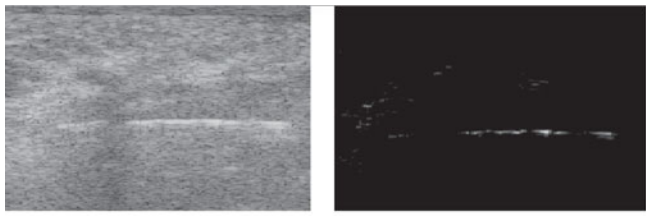

Fig. 3. Sagittal frame from *in vivo* patient data: B-mode (left) versus contrast enhanced reflected power image (right), both created from raw RF data.

was equivalent to assigning a value for each voxel (x, y, z), based on the sagittal images acquired in the polar coordinates while the probe was rotating around the z-axis. Following [20], the associated voxel value was derived from the values of its nearest neighbors between the sagittal slices by bilinear interpolation.

3) Seed Templates: Simple thresholding of the contrast enhanced RF data resulted in a large number of seed candidates and seed-like clutter. In order to reduce false positive detections, we computed the normalized cross correlation of the seed regions with seed templates. We experimented with two groups of templates: one group of templates acquired by *ex vivo* imaging of the seeds and one acquired from patient data.

Ex vivo templates: We created a set of sixteen 3-D templates each acquired by imaging a dummy seed in water at a specific orientation relative to the probe. The orientations were defined by a combination of pitch angles, $\theta_y \in \{0^\circ, 3^\circ, 6^\circ, 9^\circ\}$ and yaw angles $\theta_x \in \{0^\circ, 5^\circ, 10^\circ, 15^\circ\}$. For each of these combinations, the 3-D template was formed by rotating the probe and acquiring 21 images with the sagittal array of the transducer. An element of the data matching any of these templates was considered a seed candidate. We carried out the study of this set of seed templates because the appearance of the brachytherapy seeds within ultrasound images changes with the orientation of the seed relative to the probe. Even though the seeds are inserted by needles that are essentially in the sagittal plane of the TRUS, prostate motion due to needle forces do change this orientation.

In vivo templates: In our clinical images, the existence of background tissue, blood, and edema significantly alters the appearance of seeds in ultrasound images compared to the described *ex vivo* templates which are imaged in water, resulting in low normalized cross correlation values. Therefore, we created a second template type extracted from *in vivo* data. This template type was acquired by manually clicking the center of a visually distinct seed in 3-D *in vivo* data from one of the patients (case 2). Similar to the *ex vivo* case, the 3-D template consisted of 21 images acquired with the sagittal array of the TRUS probe as illustrated in Fig. 4. Since the appearance of the seed depends on its distance from the ultrasound transducer, templates were created from seeds at three different depth ranges. Unlike the *ex vivo* case, controlled positioning of the seeds was not possible. So, we did not have seed templates at different orientations relative to the probe.

4) NCC-Based 3-D Template Matching: The computation of the normalized cross correlation between the 3-D template g and a cropped area of the image f equal in size with g results in a new 3-D image of the same size as f, with values in range of [0,1]

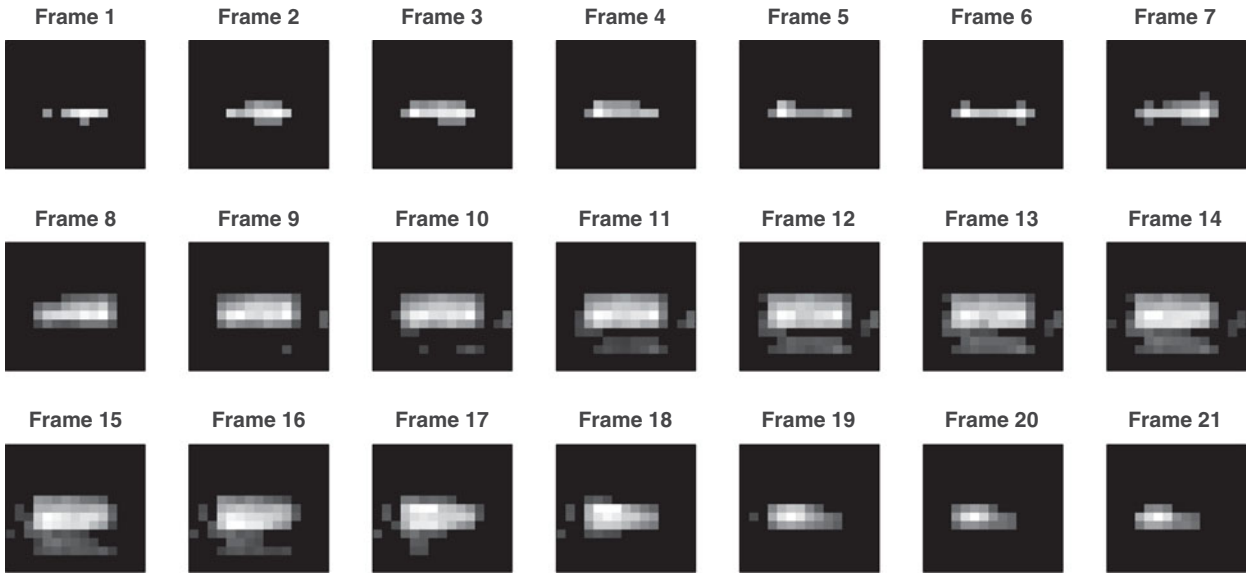

Fig. 4. 3-D seed template acquired from patient data. The frame index (1–21) corresponds to the roll angle of the sagittal array of the probe (-10 to 10°).

with largest values representing the centers of areas most similar to the template. The NCC computation can be implemented both in the frequency and the spatial domains. Lewis [21] has shown that the frequency domain implementation is faster only when the size of the template approaches the size of the image, with large template and image sizes. We found that for the specific sizes of template and image encountered in our data, the direct implementation of the numerator of the NCC formulation, using the inner product of $f' = f_{i,j,k} - \overline{f_{i,j,k}}$ and $g' = g - \overline{g}$, is more efficient than the frequency domain implementation. Note that (i, j, k) is the center of the image region f. NCC is not invariant to scale. However, in our case, the images and the templates were acquired with similar imaging parameters, therefore, the scales matched. For clinical data, NCC computation was performed using the template, among the three available templates, that was acquired at the closest depth to k.

5) Thresholding, Spatial Filtering, and Grouping in the NCC Image: The NCC image was thresholded (the reported results were obtained with threshold value of 0.3). The remaining voxels were sorted based on the NCC value. Starting from the point with the highest NCC, a neighborhood of the size of the seed was cleared around each nonzero voxel. This was necessary because each seed consists of several bright voxels, while we need a single voxel to represent the seed. It should be noted that in this approach, the voxel representing the seed is not necessarily the geometric center of the seed.

The remaining seed candidates were then divided into groups representing the needle tracks. The needle tracks in the sagittal plane were considered linear and were detected by applying the Hough transform [22] to the remaining voxels. Previous work has shown that in spite of needle deflection, in stranded brachytherapy implants, the Hough transform can isolate the seeds on individual needles as they can be parametrically modeled as an imperfect instance of a line [19]. We have followed [23] in implementing the Hough transform for detecting lines within the cluster of seeds.

Since our overall approach seeks a conservatively filtered set of seeds, we applied additional spatial filtering at this stage. We eliminated single seeds that could not be grouped into lines. Furthermore, we used our knowledge of the fixed 1 cm distance between the seeds in the stranded implants. On each needle, the seeds were sorted based on NCC values. Starting with the seed with the highest value, any other seed candidate that was within 0.8 cm was removed.

B. Matching and Registration

1) Simulating the Effect of the Ultrasound Probe on the X-ray Seed Locations: In order to avoid the obstruction of seeds by the ultrasound transducer in C-arm X-ray projections, the ultrasound probe has to be retracted or removed prior to acquisition of the C-arm images. Because during the ultrasound acquisition, it is customary to apply upward pressure on the TRUS probe, there results a deformation of the prostate posterior region compared to the C-arm acquisition. The magnitude of the deformation depends on the amount of force applied by the radiologist, through the probe holder mechanism, during imaging. In recent literature, it has been shown that the resulting deformation can be significant in some cases [24]. We used a geometric model to simulate a similar deformation on the X-ray seed cloud. We considered the posterior edge of the prostate as a segment of a tapered ellipsoid, a geometry that has been used successfully to segment the prostate gland in previous work [25], [26]. Each axial cross section of the prostate is considered to be a tapered ellipse and we assumed that the presence of the TRUS probe causes uniform deformation along the prostate. The effect of the deformation, as illustrated in a 2-D situation in Fig. 5, can be described in the polar coordinates centered at the TRUS center, as follows [25]:

$$r_e = r_w \times (1 - \sin(\theta)) e^{-r_w^2/2\sigma^2} \tag{2}$$

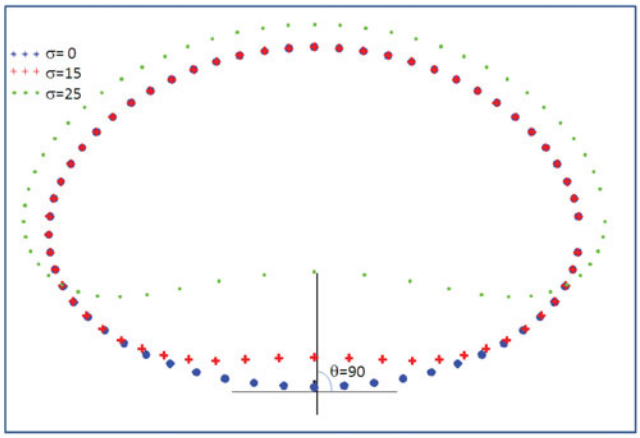

Fig. 5. Tapered ellipse, and the warped variations with $\sigma = 15$ and $\sigma = 25$.

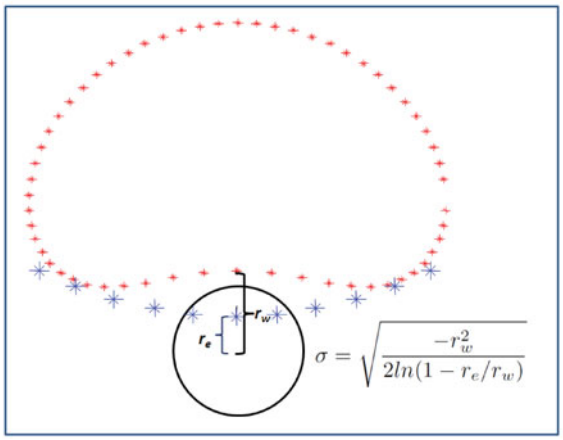

Fig. 6. Mid point of the posterior edge of the prostate gland is deformed by the TRUS probe by $r_w - r_e$.

where r_e and θ are the coordinates of a seed point prior to deformation, with $\theta = \pi/2$ being the medial line and r_w being the distance between the TRUS center and the moved seed point after applying pressure from the probe. σ is a variable that represents the magnitude of the stretch and is a function of the force exerted on the probe. Fig. 6 illustrates the relationship between σ, r_e, and r_w at $\theta = \pi/2$. This model of deformation results in maximum deformation at the contact point of the posterior wall and decreased deformation for the seeds far from the probe, or far from $\theta = \pi/2$.

In order to solve for r_w in (2) one needs to know the physical location of the ultrasound probe, and the proper value of the parameter σ. We assumed that the ultrasound probe was along the line resulting from the intersection of the sagittal mid plane of the implant and the coronal plane passing parallel to and 15 mm below the most posterior needle. This is a reasonable approximation, based on our measurements on sample axial brachytherapy images (see Fig. 7). While this value could be slightly different in different cases, a further/closer probe center is equivalent to decreased/increased probe pressure. Therefore, we worked with this reasonable assumption of the probe depth and optimized only the σ value. From phantom experiments,

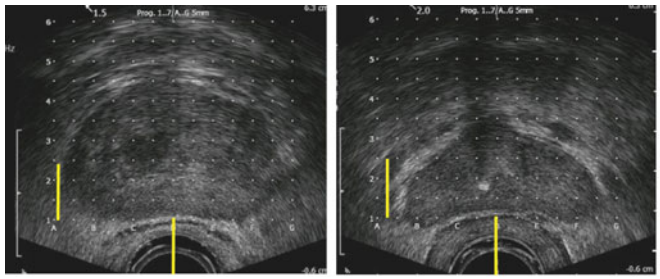

Fig. 7. Samples of the axial view of the prostate during brachytherapy, the distance between the probe center and prostate edge, marked by the yellow lines, is 14 and 15 mm in the left and the right images.

we know that applying pressure beyond what causes 1 cm of deformation at the contact point does not contribute to image quality. Therefore, we limited the search range for σ to values that would result in less than 1 cm deformation in the contact point ($r_w - r_e < 1$ cm). As the dashed link in Fig. 1 shows to determine the optimal value of the parameter σ, we created a registration loop that combines a grid search on the σ values with the registration procedure. The X-ray seed cloud was deformed according to the warping model described here, with varying values of σ resulting in deformation fields with the magnitude of 0–1 cm, with 1-mm step sizes at the assumed contact point. For each value, the two-stage registration process described in the next section was performed. The registration errors are reported for the warping parameter that minimized the registration error.

2) 2-D Matching for Initial Alignment: The partially detected seed cloud from ultrasound and the complete seed cloud from fluoroscopy were first aligned by applying a transformation that matched the centers of mass in the two clouds. To further improve the initial alignment and also to reduce the risk of local minima due to the unbalanced number of seeds in ultrasound and fluoroscopy, we performed a needle matching step to remove the needles in fluoroscopy that did not have a counterpart in ultrasound. Matching was performed by applying a 2-D rigid registration between the needle projections on the transverse plane passing through the prostate mid gland in the fluoroscopy implant. Assuming that X was the set of n projection points from ultrasound, and Y was the set of m projection points from fluoroscopy, the rotation and translation parameters of the transformation T were found to minimize $\sum_{i=1:n} d_c(T(X_i), Y)$ where $d_c(T(X_i), Y)$ is the Euclidean distance of the ultrasound projection point X_i from its closest match in the point set Y. After the matching step, the fluoroscopy needles without a match in ultrasound were removed.

3) 3-D Registration of the Seed Sets: After the matching and alignment steps, the registration problem was considered as a point set registration. Even though the change in position of the ultrasound probe from the time the 3-D ultrasound to the time the fluoro images are acquired can introduce some nonrigid deformation beyond the effect of the ultrasound probe between the ultrasound and fluoro images, due to the possible existence of outliers in the ultrasound set of seeds, the use of deformable registration could result in invalid warping. Therefore, after the warping applied to compensate the probe effect, a rigid trans-

TABLE I
CIRS PHANTOM RESULT: NUMBER OF DETECTED SEEDS, REGISTRATION ERRORS WITH ALL DETECTED NEEDLES, AND AVERAGE REGISTRATION ERROR FOR THE LEAVE-ONE-OUT VALIDATION TEST

Used Template	dist. er. (mm) all needles (ICP)	dist. er. (mm) LOO (ICP)	dist. er. (mm) all needles (GMM)	dist. er. (mm) LOO (GMM)	# fl seeds	# fl seeds, in matching needles	# of detected seeds in ultrasound
16 templates	1.6±1.3	2.3±2.6	1.7±1.2	1.7±1.2	135	110	86
Single seed template (0°,0°)	**1.6±1.2**	2.0±1.9	**1.6±1.5**	1.7±1.1	135	111	83

formation (rotation and translation) between the two sets was sought.

The Iterative Closest Point (ICP) algorithm is the most common solution for rigid point set registration [27]. However, ICP requires a fairly accurate initial alignment and is sensitive to outliers. While the matching and the 2-D registration step described earlier provides the required initial alignment, the existence of outlier points in form of false positive seeds in the ultrasound dataset is possible. Therefore, in addition to ICP, we also performed the registration of the point sets using the Gaussian mixture model (GMM) registration algorithm. In GMM, each of the point sets is represented by a mixture of Gaussian probability densities. Jian and Vemuri [28] have derived a closed form expression for the L_2 distance as a similarity measure between two probability distributions. The optimization step seeks to find the transformation parameters that minimize this L_2 norm [28].

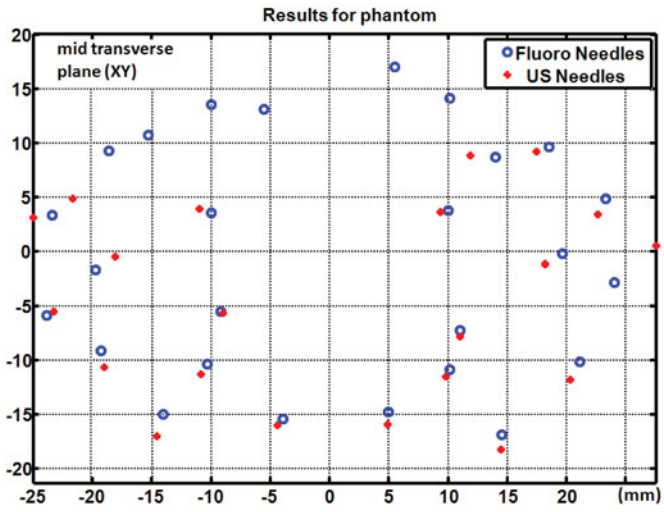

Fig. 8. *Phantom results*: 2-D matching of needle projections in the transverse plane.

III. RESULTS AND DISCUSSIONS

We quantified the outcome of the seed registration method based on the postregistration distances between ultrasound seeds and their closest fluoroscopy counterparts. We also examined the stability of needle matches and the recorded registration errors subject to the removal of any of the detected needles in a leave-one-needle-out validation step.

A. Phantom Data

Table I presents the results of ultrasound seed detection and registration for the CIRS phantom. For this experiment, the *ex vivo* templates were utilized. The first row of the table presents the results when all sixteen *ex vivo* templates were used. After all filtering steps, 86 detected ultrasound seeds remained which were grouped into 22 needles using the Hough transform. The 2-D matching outcome is illustrated in Fig. 8. The matching needles in fluoroscopy included 110 seeds. When ICP was used (see column 2, Table I), an average seed to closest seed postregistration distance of 1.6 ± 1.3 mm was obtained from the registration of the set of 86 ultrasound points to 110 fluoroscopy points. With GMM (see column 4, Table I), the outcome was not significantly different and resulted in an average distance of 1.7±1.2 mm. The deformation step had a very small effect on the registration accuracy in the phantom study. In fact, the optimal magnitude of deformation at the contact point ($r_w - r_e$) returned by the search in the range of [1 mm, 10 mm] was 1 mm and the resulting improvement in the registration accuracy compared to rigid registration was only 0.2 mm in the ICP method. This is understandable because the phantom is stiffer and the simulated rectum is straight, making it easy to acquire an image of the simulated prostate with the TRUS transducer even when very little pressure is applied.

The template matching step is time consuming. The computation time to form an NCC image equal to the size of the ultrasound data on a dual core PC 1.86 GHz, 2 GB RAM, with a MATLAB implementation, was 86 s for the template size of 30 × 60 × 21 and image size of 128 × 258 × 391. Therefore, the use of a set of sixteen templates might be prohibitive for intraoperative dosimetry. However, our experiments showed that using only the 3-D template acquired by imaging the seed at (0°, 0°) results in a similar outcome in terms of registration error. This result is provided in row two of Table I. While there is a slight decrease in the number of detected ultrasound seeds to 83, the average postregistration distance is 1.6 ± 1.2 mm using ICP and 1.6 ± 1.5 mm using GMM. In other words, we report similar registration errors both using the complete set of 3-D templates and using only one 3-D template. It is interesting to note that for both experiments, the ICP outcomes are slightly more accurate than GMM outcomes. This suggests that the initial alignment obtained from the 2-D matching step is accurate enough to trigger a successful ICP process. The sensitivity of ICP to outliers did not cause an issue in these phantom experiments, probably due to the accurate ultrasound seed detection with few false positives. Fig. 9 shows the ICP 3-D registration outcome using the detected seeds from the single template.

B. Patient Data

Table II presents the detailed results for the five patient cases. When ICP is used, the average postregistration seed distances

TABLE II
NUMBER OF THE DETECTED SEEDS, REGISTRATION ERRORS AND LEAVE ONE OUT ERRORS FOR THE FIVE PATIENT DATASETS

Case	dist. er.(mm) all needles (ICP)	dist. er. (mm) LOO (ICP)	dist. er.(mm) all needles (GMM)	dist. er.(mm) LOO (GMM)	# fl seeds	# fl seeds, in matching needles	# of detected seeds (needles) in ultrasound
Case 1	3.2±0.8	3.3±2.8	3.9±1.6	3.8±3.0	102	51	39 (13)
Case 2	2.7±0.8	3.0±1.8	3.0±1.1	3.2±1.9	122	28	12 (5)
Case 3	2.5±1.2	2.6±2.0	3.4±3.0	3.7±2.5	113	45	13 (6)
Case 4	3.1±1.2	3.5±1.6	3.2±1.9	3.4±2.0	115	76	49 (16)
Case 5	2.5±1.3	3.3±2.2	3.0±2.7	3.2±2.5	100	33	15 (5)
Average error	**2.8±1.5**	3.1±2.3	3.3±1.9	3.5±2.5			

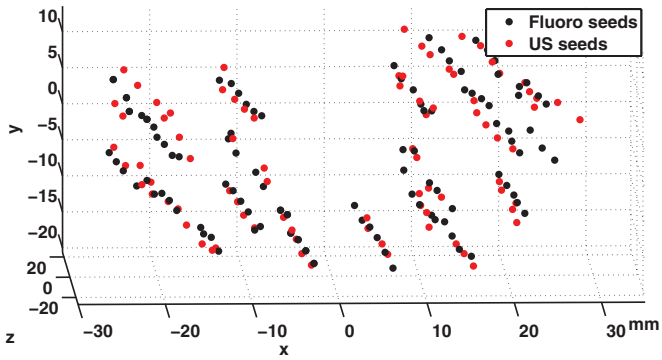

Fig. 9. *Phantom results*: 3-D registration (using ICP).

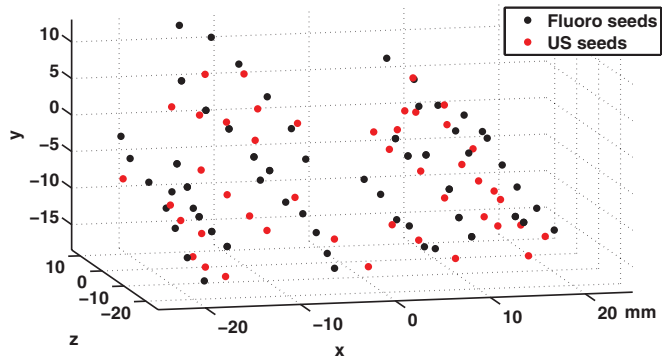

Fig. 11. Final 3-D registration result in a patient case (using ICP).

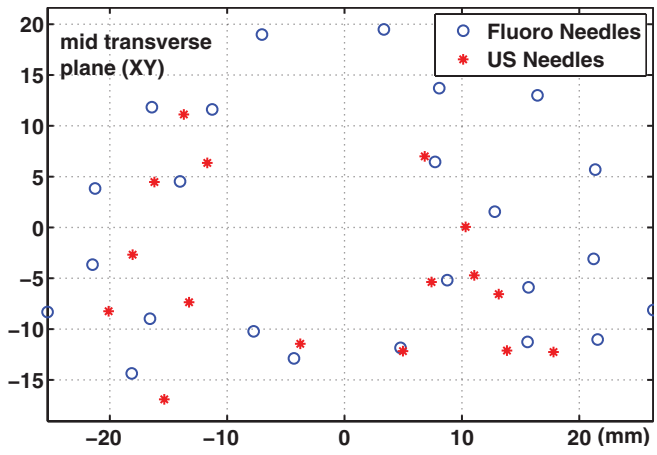

Fig. 10. Result of the initial 2-D needle matching in a patient case.

from ultrasound to fluoroscopy is 2.8 ± 1.5 mm. With GMM, the postregistration distance average is 3.3 ± 1.9 mm. There is a slight decrease in the accuracy from each ICP experiment to its counterpart GMM experiment. Even though the number of detected seeds in the patient datasets is relatively small, it appears that the 2-D matching experiment still provides an adequate initial alignment for ICP. For case 4, Figs. 10 and 11 illustrate the results of 2-D matching and 3-D registration using ICP. In both phantom and patient cases, as evident from Figs. 10 and 8, the unmatched needles tend to be from the anterior side of the prostate (top of the images), while the posterior seeds that are closest to the probe are accurately detected. This is likely due to the depth-dependent reduction in the resolution of our 3-D ultrasound system.

The effects of applying simulated deformation: The reported results in Table II were acquired with the application of the described deformation approach in the X-ray seed cloud to simulate the probe pressure effect in ultrasound. The average ICP and GMM error measurements, in the absence of the simulated deforming step, were 3.4 ± 1.7 mm and 3.9 ± 2.4 mm. The amount of improvement caused by the deforming step was 0.8, 1.4, 0.1, 0.1, and 1.4 mm in the five cases. In one case (case 2), we used the maximum of the search range for deformation $(r_w - r_e)$, which was 1 cm.

C. Leave-One-Needle-Out Validation of the Registration Process

In order to study the stability of our matching and registration procedure, we also ran a leave-one-needle-out experiment. For each patient or phantom case, assuming that n ultrasound needles were identified, we repeated the matching and registration procedure n times, each time with $n-1$ needles. This amounted to removal of three to seven (10% to 20%) of the seeds in each round for patient cases. If the registration is valid, and not just a local minimum, the removal of any specific needle should not drastically change the outcome.

This leave-one-needle-out test was performed for each template set and registration method for the phantom data (see columns 3 and 5 of Table I) and patient data (see columns 3 and 5 of Table II). For the phantom experiments, the notable result was that for the ICP registration method, the average leave-one-out result showed a deterioration in accuracy from 1.6 ± 1.2 mm to 2.0 ± 1.9 mm in the single template experiment. The GMM result, on the other hand, was robust to removal of individual needles and went from 1.6 ± 1.5 mm when all detected

needles were included to 1.7 ± 1.1 mm in the leave-one-out test. A similar pattern was witnessed when all 16 *ex vivo* templates were used. Another interesting result was that regardless of which needle was removed in the leave-one-out experiment, the matched fluoroscopy needles for the rest of ultrasound needles remained the same.

On the patient data, the average errors in the leave-one-needle-out experiment with ICP and five templates was 3.1 ± 2.3 mm, a slight increase compared to 2.8 ± 1.5 mm when all needles were included. For GMM, the leave-one-out average error was 3.5 ± 2.5 mm compared to 3.3 ± 1.9 mm with all needles included. In both methods, the leave-one-needle-out result was very close to the test that included all needles which is a sign of stability.

IV. Summary and Conclusion

We showed that it is feasible to use contrast enhanced RF ultrasound data, template matching, and spatial filtering to detect a reliable subset of brachytherapy seeds from ultrasound to enable registration to X-ray fluoroscopy. We performed point-based registration between the seed clouds from fluoroscopy and a subset of seeds detected from ultrasound images. To achieve the reliable subset of seeds needed for this purpose, we presented several technical innovations. Instead of the conventional B-mode ultrasound, we used RF signals processed to enhance seed contrast. Template matching, in the contrast enhanced RF domain, with a variety of seed templates was reported. The resulting set of seeds was also spatially filtered based on our knowledge of the fixed seed spacing in the stranded implant. To enable dosimetry, we registered the detected subset of seeds to a full reconstruction of the seed cloud in fluoroscopy. Even though the patient pose was identical between the ultrasound and fluoroscopy acquisitions, the ultrasound probe could pressure the prostate and cause deformation in ultrasound compared to X-ray images. Therefore, we simulated the effects of transducer-induced deformation on the fluoroscopy, and then registered the two seed clouds. Since the magnitude of deformation was unknown, the registration parameters and the magnitude of deformation were optimized together. We devised a two stage strategy for the rigid registration. First, the 2-D registration of needle projections from the ultrasound and fluoroscopy was performed to find a match for detected needles in ultrasound with needles in fluoroscopy. In the second step, the 3-D rigid registration of only the seeds in the matched needles was performed.

An average accuracy of 1.6 mm in phantom data and 2.8 mm in patient data was reported. An important concern for intraoperative implementation of the proposed methods is computation time. Template matching is the computational bottle neck of the methodology. However, even with the current MATLAB implementation, the template matching step is completed in 86 s for one template, and the full registration process takes between 90 and 120 s depending on the image sizes. Implementation improvements and parallelization are possible. We conclude that for institutions in which C-arm fluoroscopy is a routine part of the brachytherapy setup, the intraoperative implementation is feasible.

One source of error in registration is the fact that the seed detection algorithm is not guaranteed to return the geometric center of the seed. Also, the compensation of deformation based on the proposed method could be incomplete due to the approximations used in the applied deformation model, mainly the assumption for the location of the ultrasound probe center. In this paper, we found large non-rigid deformations in two of the five patient cases. To accurately measure the percentage of such cases and the effectiveness of the applied deformation field we need a larger patient cohort. Another source of error is that the 3-D ultrasound system used in this paper acquired sagittal images while rotating radially. This causes a decrease in the spatial resolution at increasing distances from the probe. The result was the detection of fewer seeds far from the probe. Addressing this depth-dependent image quality issue and improving the overall image quality by increasing the line density are among future modifications to the protocol. Another modification is to acquire ultrasound images after only a part of the implant, for example, the anterior row of needles, is inserted. This will decrease the shadowing effects which reduce ultrasound image quality. It should also be noted that the limitations of correlation-based measures for template matching are well documented [29]. While moving beyond this feasibility work we will use more advanced techniques for template matching.

Data from the five clinical cases show that our technique is a potentially powerful tool for dosimetry when ultrasound and C-arm imaging are available. Real-time dosimetry and the study of the impact of plan modification based on intraoperative dosimetry on patient outcome is among our current research goals.

Acknowledgment

The authors would like to thank Dr. T. Pickles, Dr. M. McKenzie, Dr. N. Chng, Dr. Xu Wen, and the staff of Vancouver Cancer Center.

References

[1] W. J. Morris, M. Keyes, D. Palma, I. Spadinger, M. R. McKenzie, A. Agranovich, T. Pickles, M. Liu, W. Kwan, J. Wu, E. Berthelet, and H. Pai, "Population-based study of biochemical and survival outcomes after permanent 125I brachytherapy for low- and intermediate-risk prostate cancer," *Urology*, vol. 73, no. 4, pp. 860–865, 2009.

[2] P. F. Orio, I. B. Tutar, S. Narayanan, S. Arthurs, P. S. Cho, Y. Kim, G. Merrick, and K. E. Wallner, "Intraoperative ultrasound-fluoroscopy fusion can enhance prostate brachytherapy quality," *Int. J. Radiat Oncol Biol. Phys.*, vol. 69, no. 1, pp. 302–307, Sep. 2007.

[3] A. Polo, C. Salembier, J. Venselaar, and P. Hoskin, "Review of intraoperative imaging and planning techniques in permanent seed prostate brachytherapy," *Radiotherapy Oncol.*, vol. 94, pp. 12–23, 2010.

[4] Y. Yu, S. T. Acton, and K. Thornton, "Detection of radioactive seeds in ultrasound images of the prostate," in *Proc. IEEE Int. Conf. Image Process.*, Oct. 2001, vol. 2, pp. 319–322.

[5] J. Mamou, S. Ramachandran, and E. J. Feleppa, "Angle-dependent ultrasonic detection and imaging of brachytherapy seeds using singular spectrum analysis," *J. Acoust. Soc. Amer.*, vol. 123, no. 4, pp. 2148–2159, 2008.

[6] M. Ding, L. Gardi, Z. Wei, and A. Fenster, "3D TRUS image segmentation in prostate brachytherapy," in *Conf. Proc. IEEE Eng. Med. Biol. Soc.*, 2005, vol. 7, pp. 7170–7173.

[7] S. A. McAleavey, D. J. Rubens, and K. J. Parker, "Doppler ultrasound imaging of magnetically vibrated brachytherapy seeds," *IEEE Trans. Biomed. Eng.*, vol. 50, no. 2, pp. 252–255, Feb. 2003.

[8] A. K. Jain, Y. Zhou, T. Mustufa, E. C. Burdette, G. S. Chirikjian, and G. Fichtinger, "Matching and reconstruction of brachytherapy seeds using the hungarian algorithm (MARSHAL)," *SPIE Med. Imag.*, vol. 5744, pp. 810–821, 2005.
[9] P. Fallavollita, Z. K. Aghaloo, E. C. Burdette, D. Y. Song, P. Abolmaesumi, and G. Fichtinger, "Registration between ultrasound and fluoroscopy or CT in prostate brachytherapy," *Med. Phys.*, vol. 37, no. 6, pp. 2749–2760, Jun. 2010.
[10] D. French, J. Morris, M. Keyes, and S. Salcudean, "Real-time dosimetry for prostate brachytherapy using TRUS and fluoroscopy," in *Medical Image Computing and Computer-Assisted Intervention* (Lecture Notes in Computer Science Series), vol. 3217, Berlin, Germany: Springer, 2004, pp. 983–991.
[11] Y. Su, B. J. Davis, K. M. Furutani, M. G. Herman, and R. A. Robb, "Seed localization and TRUS-fluoroscopy fusion for intraoperative prostate brachytherapy dosimetry," *Comput. Aided Surg.*, vol. 12, no. 1, pp. 25–34, Jan. 2007.
[12] D. A. Todor, M. Zaider, G. N. Cohen, M. F. Worman, and M. J. Zelefsky, "Intraoperative dynamic dosimetry for prostate implants," *Phys. Med. Biol.*, vol. 48, pp. 1153–1171, 2003.
[13] V. Singh, L. Mukherjee, J. Xu, K. R. Hoffmann, P. M. Dinu, and M. Podgorsak, "Brachytherapy seed localization using geometric and linear programming techniques," *IEEE Trans. Med. Imag.*, vol. 26, no. 9, pp. 1291–1304, Sep. 2007.
[14] Y. Su and R. Robb, "Seed image reconstruction using a template matching technique," in *SPIE Med. Imag.*, 2005, vol. 5747, pp. 1038–1045.
[15] E. Dehghan, J. Lee, M. Moradi, X. Wen, G. Fichtinger, and S. E. Salcudean, "Prostate brachytherapy seed reconstruction using C-arm rotation measurement and motion compensation," in *Medical Image Computing and Computer-Assisted Intervention* (Lecture Notes in Computer Science Series), vol. 6361. Berlin, Germany: Springer, 2010, pp. 283–290.
[16] M. Zhang, M. Zaider, M. Worman, and G. Cohen, "On the question of 3D seed reconstruction in prostate brachytherapy: The determination of x-ray source and film locations," *Phys. Med. Biol.*, vol. 49, no. 19, pp. N335–N345, Oct. 2004.
[17] I. B. Tutar, L. Gong, S. Narayanan, S. D. Pathak, P. S. Cho, K. Wallner, and Y. Kim, "Seed-based transrectal ultrasound-fluoroscopy registration method for intraoperative dosimetry analysis of prostate brachytherapy," *Med. Phys.*, vol. 35, no. 3, pp. 840–848, Mar. 2008.
[18] N. Chng, I. Spadinger, W. J. Morris, N. Usmani, and S. Salcudean, "Prostate brachytherapy postimplant dosimetry: Automatic plan reconstruction of stranded implants," *Med. Phys.*, vol. 38, no. 1, pp. 327–342, Jan. 2011.
[19] X. Wen, S. T. E. Salcudean, and P. D. Lawrence, "Detection of brachytherapy seeds using 3-D transrectal ultrasound," *IEEE Trans. Biomed. Eng.*, vol. 57, no. 10, pp. 2467–2477, Oct. 2010.
[20] S. Tong, D. B. Downey, H. N. Cardinal, and A. Fenster, "A three dimensional ultrasound prostate imaging system," *Ultrasound Med. Biol.*, vol. 22, pp. 735–746, 1996.
[21] J. P. Lewis, "Fast template matching," in *Proc. Vision Interface CIPPRS*, 1995, pp. 120–123.
[22] R. O. Duda and P. E. Hart, "Use of the Hough transformation to detect lines and curves in pictures," *Commun. ACM*, vol. 15, pp. 11–15, 1972.
[23] R. Ebrahimi, S. Okazawa, R. Rohling, and S. E. Salcudean, "Hand-held steerable needle device," in *Medical Image Computing and Computer-Assisted Intervention* (Lecture Notes in Computer Science Series). Berlin, Germany: Springer, 2003, pp. 223–230.
[24] E. Dehghan, J. Lee, P. Fallavollita, N. Kuo, A. Deguet, E. C. Burdette, D. Y. Song, J. L. Prince, and G. Fichtinger, "Point-to-volume registration of prostate implants to ultrasound," in *Medical Image Computing and Computer-Assisted Intervention* (Lecture Notes in Computer Science Series), vol. 6892. Berlin, Germany: Springer, 2011, pp. 615–622.
[25] S. Badiei, S. E. Salcudean, J. Varah, and W. J. Morris, "Prostate segmentation in 2D ultrasound images using image warping and ellipse fitting," in *Medical Image Computing and Computer-Assisted Intervention* (Lecture Notes in Computer Science Series), vol. 4191. Berlin, Germany: Springer, 2006, pp. 17–24.
[26] S. S. Mahdavi, N. Chng, I. Spadinger, W. J. Morris, and S. E. Salcudean, "Semi-automatic segmentation for prostate interventions," *Med. Image Anal.*, vol. 15, no. 2, pp. 226–237, 2011.
[27] P. J. Besl and N. D. McKay, "A method for registration of 3-D shapes," *IEEE Trans. Pattern Anal. Mach. Int.*, vol. 14, no. 2, pp. 239–256, Feb. 1992.
[28] B. Jian and B. C. Vemuri, "A robust algorithm for point set registration using mixture of Gaussians," in *Proc. IEEE Int. Conf. Comput. Vis.*, Oct. 2005, vol. 2, pp. 1246–1251.
[29] R. Brunelli and T. Poggio, "Template matching: Matched spatial filters and beyond," *Pattern Recogn.*, vol. 30, pp. 751–768, 1997.

Mehdi Moradi (SM'02–M'09) received the B.Sc. degree in biomedical engineering from Tehran Polytechnic, the M.Sc. degree in electrical engineering from the University of Tehran, and the Ph.D. degree in biomedical computing from Queen's University, Kingston, ON, Canada, in 2008.

He has worked as an NSERC Postdoctoral Fellow at the University of British Columbia (2009–2011) and as a Research Scientist at Harvard Medical School (2011–2012). He joined the Department of Electrical and Computer Engineering at the University of British Columbia as an Assistant Professor in 2012. His broad research interests include machine learning in medical image analysis, image-guided therapy and diagnosis, and multimodality and multiparametric imaging.

S. Sara Mahdavi (S'08) received the B.Sc. degree from the Sharif University of Technology, Tehran, Iran, in 2004, and the M.Sc. degree from Tehran University, Tehran, Iran, in 2007, both in electrical engineering. She is currently working toward the Ph.D. degree in the Department of Electrical and Computer Engineering, University of British Columbia, Vancouver, Canada.

He is also a Research Assistant in the Robotics and Control Laboratory, Department of Electrical and Computer Engineering, University of British Columbia. Her research interests include image analysis and computer-aided medical interventions.

Ehsan Dehghan received the B.Sc. and M.Sc. degrees in electrical engineering from the Sharif University of Technology, Tehran, Iran, in 2001 and 2003, respectively, and the Ph.D. degree in electrical and computer engineering from the University of British Columbia, Vancouver, BC, Canada, in 2009.

From 2009 to 2012, he was a Postdoctoral Fellow at the Queen's University, Kingston, ON, Canada, and the Johns Hopkins University, Baltimore, MD. He is currently with Philips Research North America, Briarcliff Manor, NY. His research interests include image-guided and computer-assisted interventions, medical image analysis, soft tissue modeling and simulation, medical robotics, finite element modeling, and control systems.

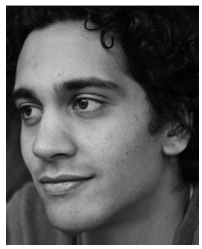

Julio R. Lobo received the B.A.Sc. degree in engineering physics from the University of British Columbia, Vancouver, Canada, in 2010, where He is currently working toward the M. Sc. degree in electrical engineering. He completed a Research Studentship at the British Columbia Cancer Agency in 2009.

His previous research interests include the Monte Carlo simulations of dynamic radiotherapy treatment techniques and reconstruction and registration algorithms for prostate brachytherapy. His current research interests include intraoperative dosimetry and ultrasound elastography for prostate brachytherapy.

Sanchit Deshmukh is currently working toward the B.Tech. and M.Tech. (Microelectronics) degrees at the Department of the Electrical Engineering, Indian Institute of Technology, Bombay, India, where his Master's thesis is focused on modeling resistive memory devices.

He contributed to research on ultrasound imaging for brachytherapy at the University of British Columbia, Vancouver, Canada, in 2010, and on memory hardware optimizations at the Centre for Silicon Systems Implementation (CSSI), Carnegie Mellon University in 2011.

William James Morris received the M.D. degree from the University of British Columbia, Canada, in 1985.

He is a Radiation Oncologist at British Columbia Cancer Agency and one of the Founders and the Former Head during 1997–2008 of the British Columbia Provincial Prostate Brachytherapy Program which is the largest prostate brachytherapy program in Canada having done more than 4000 implants to date. He and his colleagues have published more than 50 refereed publications and have presented dozens of abstracts at national and international meeting detailing various aspects of brachytherapy for prostate cancer. He is the Principle Investigator for developmental brachytherapy at the Vancouver Cancer Centre, Vancouver, Canada.

He is currently the Chair of the Brachytherapy Quality Assurance Committee.

Gabor Fichtinger (M'04) received the Ph.D. degree in computer science from the Technical University of Budapest, Budapest, Hungary, in 1990.

He is currently a Professor in the School of Computing, with cross appointments in the Departments of Mechanical and Material Engineering, Electrical and Computer Engineering, and Surgery, Queen's University, Kingston, ON, Canada, where he directs the Percutaneous Surgery Laboratory. His research specializes on medical image computing and computer-assisted interventions, primarily for the diagnosis, and therapy of cancer.

Dr. Fichtinger holds a Level-1 Cancer Care Ontario Research Chair in Cancer Imaging.

Septimiu (Tim) E. Salcudean (S'78–M'79–SM'03–F'05) received the B.Eng. (Hons.) and M.Eng. degrees from McGill University, Montreal, QC, Canada, and the Ph.D. degree from the University of California, Berkeley, all in electrical engineering.

From 1986 to 1989, he was a Research Staff Member in the robotics group at the IBM Thomas J. Watson Research Center, Yorktown, NY. He then joined the Department of Electrical and Computer Engineering, University of British Columbia, Vancouver, BC, Canada, where he is currently a Professor and holds a Canada Research Chair and the C. A. Laszlo Chair in biomedical engineering. Between 1996 and 1997, he was at ONERA-CERT, Toulouse, France, an Aerospace-Controls Laboratory, where he received a Killam Research Fellowship. In 2005, he spent six months in the Medical Robotics Group, Centre National de la Recherche Scientifique, Grenoble, France. He has been a Co-Organizer of several symposia on haptic interfaces. His research interests include medical robotics and ultrasound image guidance, elastography, medical simulation, and virtual environments.

Dr. Salcudean is a Fellow of the Canadian Academy of Engineering. He was a Technical and a Senior Editor of the IEEE TRANSACTIONS ON ROBOTICS AND AUTOMATION.